Inertial focusing of finite-size particles in microchannels

By Evgeny S. Asmolov[1,2]†, Alexander L. Dubov[1], Tatiana V. Nizkaya[1], Jens Harting[2,3,4], and Olga I. Vinogradova[1,5,6]‡

[1]A.N. Frumkin Institute of Physical Chemistry and Electrochemistry,
Russian Academy of Sciences, 31 Leninsky Prospect, 119071 Moscow, Russia

[2]Institute of Mechanics, M. V. Lomonosov Moscow State University, 119991 Moscow, Russia

[3]Helmholtz Institute Erlangen-Nürnberg for Renewable Energy, Forschungszentrum Jülich, Fürther Str. 248, 90429 Nürnberg, Germany

[4]Department of Applied Physics, Eindhoven University of Technology, PO box 513, 5600MB Eindhoven, The Netherlands

[5] Faculty of Science and Technology, University of Twente, 7500 AE Enschede, The Netherlands

[6]Department of Physics, M. V. Lomonosov Moscow State University, 119991 Moscow, Russia

[7]DWI - Leibniz Institute for Interactive Materials, Forckenbeckstr. 50, 52056 Aachen, Germany

(Received Received: date / Accepted: date)

At finite Reynolds numbers, Re, particles migrate across laminar flow streamlines to their equilibrium positions in microchannels. This migration is attributed to a lift force, and the balance between this lift and gravity determines the location of particles in channels. Here we demonstrate that velocity of finite-size particles located near a channel wall differs significantly from that of an undisturbed flow, and that their equilibrium position depends on this, referred to as slip velocity, difference. We then present theoretical arguments, which allow us to generalize expressions for a lift force, originally suggested for some limiting cases and $\mathrm{Re} \ll 1$, to finite-size particles in a channel flow at $\mathrm{Re} \leq 20$. Our theoretical model, validated by lattice Boltzmann simulations, provides considerable insight into inertial migration of finite-size particles in microchannel and suggests some novel microfluidic approaches to separate them by size or density at a moderate Re.

1. Introduction

Microfluidic systems have been shown to be very useful for continuous manipulation and separation of microparticles with increased control and sensitivity, which is important for a wide range of applications in chemistry, biology, and medicine. Traditional microfluidic techniques of particle manipulation rely on low Reynolds number laminar flow. Under these conditions, when no external forces are applied, particles follow fluid streamlines. Contrary to this, particles migrate across streamlines to some stationary positions in microchannels when inertial aspects of the flow become significant. This migration is attributed to inertial lift forces, which are currently successfully used in microfluidic systems to focus and separate particles of different sizes continuously, at high flow rate, and without external forces (Di Carlo *et al.* 2007; Bhagat *et al.* 2008). The rapid development of inertial microfluidics has raised a considerable interest in the

† Email address for correspondence: aes50@yandex.ru
‡ Email address for correspondence: oivinograd@yahoo.com

lift forces on particles in confined flows. We mention below what we believe are the most relevant contributions.

Inertial lift forces on neutrally buoyant particles have been originally reported for macroscopic channels (Segré & Silberberg 1962). This pioneering work has concluded that particles focus to a narrow annulus at radial position 0.6 of a pipe radius, and argued that lift forces vanish at this equilibrium position. However, no particle manipulation systems have been explored based on macroscale systems. Much later this inertial focusing has provided the basis for various methods of particle separation by size or shape in microfluidics devices (see Martel & Toner (2014) and Zhang *et al.* (2016) for recent reviews). In these microfluidic applications the inertial lift has been balanced by the Dean force due to a secondary rotational flow caused by inertia of the fluid itself, which can be generated in curved channels (Bhagat *et al.* 2008). These Dean drag forces alter equilibrium positions of particles. The preferred location of particles in microchannels could also be controlled by the balance between inertial lift and external forces, such as electric (Zhang *et al.* 2014) or magnetic (Dutz *et al.* 2017).

In recent years extensive efforts have gone into experimental investigating particle equilibrium positions in cylindrical (Matas *et al.* 2004; Morita *et al.* 2017) and rectangular channels (Choi *et al.* 2011; Miura *et al.* 2014; Hood *et al.* 2016). Matas *et al.* (2004) have shown that the Segré-Silberberg annulus for neutrally-buoyant particles shifts toward the wall as Re increases and toward the pipe center as particle size increases. At large $\mathrm{Re} \geq 600$, some particles accumulate in an inner annulus near the pipe centre. Morita *et al.* (2017) have found that the inner annulus is not a true equilibrium position, but a transient zone, and that in a long enough pipe all particles accumulate within the Segré-Silberberg annulus. It has also been found that equilibrium positions of slightly non neutrally-buoyant particles in a horizontal pipe are shifted toward a pipe bottom (Matas *et al.* 2004).

During last several years numerical calculations (Di Carlo *et al.* 2009; Liu *et al.* 2015; Loisel *et al.* 2015) and computer simulations (Chun & Ladd 2006; Kilimnik *et al.* 2011) have also been concerned with phenomena of the inertial migration. It has been shown that in rectangular channels particles initially migrate rapidly to manifolds, and then slowly focus within the manifolds to stable equilibrium positions near wall centers and channel corners (Chun & Ladd 2006; Di Carlo *et al.* 2009; Hood *et al.* 2016). There could be two, four or eight equilibrium positions depending on the particle size, channel aspect ratio and Reynolds number. Overall, simulations are consistent with experimental results (Choi *et al.* 2011; Miura *et al.* 2014; Hood *et al.* 2016).

There is also a large literature describing attempts to provide a theory of inertial lift. An asymptotic approach, which can shed light on these phenomena, has been developed by several authors (Saffman 1965; Ho & Leal 1974; Vasseur & Cox 1976; Cox & Hsu 1977; Schonberg & Hinch 1989; Asmolov 1999; Matas *et al.* 2004, 2009). Most papers have considered a plane Poiseuille flow except the work by Matas *et al.* (2009) where a pipe flow has been addressed. The approach can be applied when the particle Reynolds number, $\mathrm{Re}_p = a^2 G/\nu$, where a is the particle radius, G is the characteristic shear rate and ν is the kinematic viscosity, is small. If so, to the leading order in Re_p, the disturbance flow is governed by the Stokes equations, and a spherical particle experiences a drag and a torque, but no lift. The Stokeslet disturbance originates from the particle translational motion relative to the fluid and is proportional to the slip velocity $V_s' = V' - U'$, where V' and U' are forward velocities of the particle and of the undisturbed flow at the particle center. The stresslet is induced by free rotation of the sphere in the shear flow and is proportional to G. The lift force has then been deduced from the solution of the next-order equations which accounts a non-linear coupling between the two disturbances (Vasseur & Cox 1976):

$$F_l' = \rho a^2 \left(c_{l0} a^2 G^2 + c_{l1} a G V_s' + c_{l2} V_s'^2 \right), \tag{1.1}$$

where ρ is the fluid density. The coefficients c_{li} $(i = 0, 1, 2)$ generally depend on several di-

mensionless parameters, such as z/a, H/a, V_s'/U_m', and on the channel Reynolds number, $\mathrm{Re} = U_m'H/\nu$, where z is the distance to the closest wall, H is the channel thickness, and U_m' is the maximum velocity of the channel flow. Solutions for c_l have been obtained in some limiting cases only, and no general analytical equations have still been proposed for finite-sized particles in the channel. Thus, Vasseur & Cox (1976) have calculated the coefficients $c_{l0}^{VC}, c_{l1}^{VC}, c_{l2}^{VC}$ for pointlike particles at small channel Reynolds numbers, $\mathrm{Re} \ll 1$, which depend on z/H only and are applicable when $z \gg a$. Cherukat & Mclaughlin (1994) have later evaluated the coefficients $c_{li}^{CM}(z/a)$ for finite-size particles near a single wall in a linear shear flow assuming that $z \sim a$ and proposed simple fits for them. However, it remains unclear if and how earlier theoretical results for pointlike particles at $\mathrm{Re} \ll 1$ or for finite-size particles near a single wall can be generalized to predict the lift of finite-size particles at any z and a finite Re of a microfluidic channel.

According to Equation (1.1) the contribution of the slip velocity to the lift forces dominates when $V_s' \gg Ga$. Since the slip velocity is induced by external forces, such as gravity, it is believed that it impacts a hydrodynamic lift only in the case of non-neutrally buoyant particles. For neutrally buoyant particles with equal to ρ density, the slip velocity is normally considered to be negligibly small (Ho & Leal 1974; Hood *et al.* 2015). A corollary from that would be that the lift of neutrally buoyant particles could be due to the stresslet only. Such a conclusion, however, can be justified theoretically only for small particles far from walls, $z \gg a$, but hydrodynamic interactions at finite distances $z \sim a$ can induce a finite slip, $V_s' \sim Ga$, so that all terms in Equation (1.1) become comparable (Cherukat & Mclaughlin 1994). The variation of the slip velocity of neutrally buoyant particles in a thin near-wall layer can impact the lift force, but we are unaware of any previous work that has addressed this question.

The purpose of this introduction has been to show that, in spite of its importance for inertial microfluidics, the lift forces of finite-size particles in a bounded geometry of a microchannel still remain poorly understood. In particular, there is still a lack of simple analytical formulas quantifying the lift, as well as of general solutions valid in the large range of parameters typical for real microfluidic devices. Given the current upsurge of interest in the inertial hydrodynamic phenomena and their applications to separation of particles in microfluidic devices it would seem timely to provide a more satisfactory theory of a hydrodynamic lift in a microchannel and also to bring some of modern simulation techniques to bear on this problem. In this paper we present some results of a study of a migration of finite-size particles at moderate channel Reynolds numbers, $\mathrm{Re} \sim 10$, with the special focus on the role of the slip velocity in the hydrodynamic lift.

Our paper is arranged as follows. In §2 we propose a general expression for the lift force on a neutrally buoyant particle in a microchannel, which reduces to earlier theoretical results (Vasseur & Cox 1976; Cherukat & Mclaughlin 1994) in relevant limiting cases. We also extend our expression to the case of slightly non-neutrally buoyant particles with the slip velocity smaller than $G_m a$. To access the validity of the proposed theory we use a simulation method described in §3, and the numerical results are presented in §4. We conclude in §5 with a discussion of our results and their possible relevance for a fractionation of particles in microfluidic devices. Appendices A and B contain a summary of early calculations of lift coefficients and the derivation of differential equations that determine trajectories of particles.

2. Theory

In this section we propose an analytical expression for the lift force on neutrally buoyant and slightly non-neutrally buoyant particles of radius a, which translate parallel to a channel wall. Our expression is valid for $a/H \ll 1$ at any distance z from the channel wall.

We consider a pressure-driven flow in a flat inclined microchannel of thickness H. An inclination angle $\alpha \geq 0$ is defined relative to the horizontal. The coordinate axis x is parallel to the

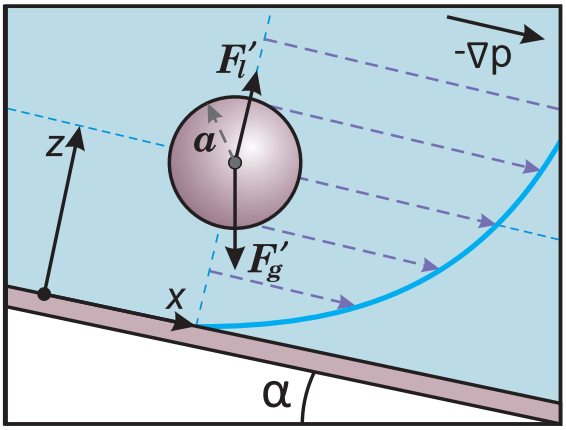

FIGURE 1. Sketch of a migration of a particle of radius a to an equilibrium position in a pressure-driven flow. The locus of this position is determined by the balance between lift, F_l', and gravity, F_g', forces.

channel wall, and the normal to the wall coordinate is denoted by z. The geometry is shown in Figure 1. The undisturbed velocity profile in such a channel is given by

$$U'(z) = 4U_m' z(1 - z/H)/H. \tag{2.1}$$

Let us now introduce a dimensionless slip velocity $V_s = V_s'/(aG_m)$, where $G_m = 4U_m'/H$ is the maximum shear rate at the channel wall. We can then rewrite Equation (1.1) as

$$F_l' = \rho a^4 G_m^2 c_l, \tag{2.2}$$

with the lift coefficient

$$c_l = c_{l0} + c_{l1} V_s + c_{l2} V_s^2, \tag{2.3}$$

which depends on the slip velocity, V_s, which in turns can be determined from the Stokes equations (a zero-order solution). Therefore, to construct a general expression for a lift force acting on finite size particles in the channel it is necessary to estimate V_s as a function of z.

We begin by studying the classical case of neutrally buoyant (i.e. force- and a torque-free) particles with a density ρ_p equal to that of liquid, ρ. The expression for V_s in a linear shear flow near a single wall has been derived before (Goldman *et al.* 1967) and can be used to calculate the slip velocity in the near-wall region of our channel. The fits for V_s are given in Appendix A, Equations (A 2)-(A 4). We first note that depending on z/a one can distinguish between two different regimes of behavior of V_s. In the central part of the channel, i.e. when $z/a \gg 1$, the slip contribution to the lift decays as $(a/z)^3$ (Wakiya *et al.* 1967), being always very small, but finite. In contrast, when the gap between the sphere and the wall is small, $z/a - 1 \ll 1$, the slip velocity varies very rapidly with z/a (Goldman *et al.* 1967):

$$V_s^{nb} = -1 + \frac{0.7431}{0.6376 - 0.200 \log(z/a - 1)}. \tag{2.4}$$

As a side note we should like to mention here that a logarithmic singularity in Equation (2.4) implies that in the near-wall region the lift coefficient, Equation (2.3), cannot be fitted by any power law $(a/z)^n$ as it has been previously suggested (Di Carlo *et al.* 2009; Hood *et al.* 2015; Liu *et al.* 2016).

It follows from Equation (2.4) that for an immobile particle in a contact with the wall, $z = a$, the slip velocity is largest, $V_s = -1$. In this limiting case the lift coefficient also takes its maximum value, $c_l^{KL} \simeq 9.257$ (Krishnan & Leighton Jr. 1995). Far from the wall, the slip velocity is much

smaller and can be neglected, so that we can consider $c_l \simeq c_{l0}$. Therefore, when $a \ll z \ll H$, the value of c_l in Equation (2.3) is equal to $c_{l0}^{CV}|_{z/H\to 0} = 55\pi/96 \simeq 1.8$ (Cox & Hsu 1977), i.e. it becomes much smaller than for a particle at the wall. This illustrates that c_l varies significantly in the vicinity of the wall due to a finite slip.

We now remark that the Stokeslet contribution (the second and the third terms in Equation (2.3)) is finite for $z \sim a$ only and vanishes in the central part of the channel. Within the close proximity to the wall we may neglect the corrections to the slip and the lift of order a/H due to parabolic flow (Pasol *et al.* 2006; Yahiaoui & Feuillebois 2010) and due to the second wall. Therefore, in this region one can use the results by Cherukat & Mclaughlin (1994) for the lift coefficients c_{li}^{CM}. The stresslet contribution to the lift (first term in Equation (2.3)) is finite for any z. Close to the wall, the effect of particle size for this term is negligible as the coefficient $c_{l0}^{CM}(z/a)$ is nearly constant (Cherukat & Mclaughlin 1994). So we may describe the stresslet contribution by the coefficient c_{l0}^{VC} obtained by Vasseur & Cox (1976). This enables us to construct the following formula for the lift coefficient:

$$c_l = c_{l0}^{VC}(z/H) + \gamma c_{l1}^{CM}(z/a)V_s + c_{l2}^{CM}(z/a)V_s^2, \tag{2.5}$$

where $\gamma = G(z)/G_m = 1 - 2z/H \leq 1$ is a dimensionless local shear rate at the particle position. The fitting expressions for three lift coefficients are summarized in Appendix A. We, therefore, use Equation (A 6) to calculate c_{l0}^{VC}, Equation (A 9) to calculate c_{l1}^{CM}, and Equation (A 10) for c_{l2}^{CM}. Note that in the second term of Equation (2.5) we have introduced a correction factor γ, which takes into account the variation of G in the second term of Equation (1.1) and ensures the lift to remain zero at the channel centerline.

We recall, that Equation (2.5) is asymptotically valid for any z when $a/H \ll 1$ and $\mathrm{Re} \ll 1$. However, one can argue that it should be accurate enough at moderate Reynolds numbers. Indeed, the contribution of undisturbed flow to inertial terms in the Navier-Stokes equations remains relatively small when $\mathrm{Re} \leq 20$. By this reason constructed for $\mathrm{Re} \ll 1$ regular-perturbation methods (Ho & Leal 1974; Vasseur & Cox 1976; Cherukat & Mclaughlin 1994) have successfully predicted the lift force on a point-like neutrally buoyant particle at a moderate Re. For larger Re, when a contribution of inertial terms becomes significant, the equilibrium positions should be shifted towards the wall with the increase in Re (Schonberg & Hinch 1989; Asmolov 1999).

We now turn to non-neutrally buoyant particles, which density is different from that of liquid, so that they experience an external gravity force, F_g', which in dimensionless form can be expressed as

$$F_g = \frac{F_g'}{\rho a^4 G_m^2} = \frac{4\pi g}{3aG_m^2}\Delta\rho, \tag{2.6}$$

where $\Delta\rho = (\rho_p - \rho)/\rho$. The gravity influences both the particle migration and equilibrium position when $F_g = O(1)$. It also induces an additional slip velocity which is of the order of the Stokes settling velocity,

$$V^{St} = \frac{F_g'}{6\pi\mu a^2 G_m} = \frac{\mathrm{Re}_p F_g}{6\pi}, \tag{2.7}$$

where μ is the dynamic viscosity. The effect of this velocity on the lift is comparable to F_l^{nb} when $V^{St} = O(1)$, i.e., at large gravity, $F_g \sim 6\pi\mathrm{Re}_p^{-1} \gg 1$, and is very important for vertical or nearly vertical channels. For horizontal channels, the slip velocity is equal to that of a neutrally buoyant sphere since $F_x = 0$. Equation (2.5) can also be applied in this case since the slip velocity remains small far from walls. Equilibrium positions of particles, z_{eq}, can then be deduced from the balance between the lift and the gravity,

$$c_l(z_{eq}) = F_g. \tag{2.8}$$

Equation(2.8) may have two, one or no stable equilibrium points depending on F_g, and the sensitivity of equilibrium positions to the value of a or $\Delta\rho$ is defined by the value $\partial c_l/\partial z$. Thus, when the derivative is small, small variations in F_g will lead to a significant shift in focusing positions. We finally note that the range of possible z_{eq} can be tuned by the choice of U'_m.

3. Simulation method

In this section, we present our simulation method and justify the choice of parameters.

For our computer experiment, we chose a scheme based on the lattice Boltzmann method (Benzi *et al.* 1992; Kunert *et al.* 2010; Dubov *et al.* 2014) which has been successfully employed earlier to simulate a motion of particles in the channel flow. We use a simulation cell confined by two impermeable no-slip walls located at $z = 0$ and $z = 79\delta$, so that in all simulations $H = 79\delta$, and two periodic boundaries with $N_x = N_y = 256\delta$, where δ is the lattice spacing. Spherical particles of radii $a = 4\delta - 12\delta$ are implemented as moving no-slip boundaries (Ladd & Verberg 2001; Janoschek *et al.* 2010; Harting *et al.* 2014), where the chosen radii are sufficient to keep discretisation effects of the order of a few percent (Janoschek 2013). A Poiseuille flow is generated by applying a body force, which is equivalent to a pressure gradient $-\nabla p$. We use a 3D, 19 velocity, single relaxation time implementation of the lattice Boltzmann method, where the relaxation time τ is kept to 1 throughout this paper. Different flow rates are obtained by changing the fluid forcing. We use two channel Reynolds numbers, $\mathrm{Re} = 11.3$ and 22.6. To simulate the migration in an inclined channel we apply the gravity force directed at an angle α relative to the z-axis at the center of the particle. In our simulations the values of dimensionless F_g vary from 0 (neutrally buoyant particle) to 13.91.

In our computer experiments we determine the lift by using two different strategies. In the first method we extract the lift from the migration velocity. We measure the $x-$ and $z-$components of the particle velocity to find the dimensionless slip, $V_s = (V'_x - U'(z))/(aG_m)$, and migration velocities, $V_m = V'_z/(aG_m)$. To suppress the fluctuations arising from the discretization artifacts we average the velocities over approximately 4000 timesteps. The error does not exceed 3% for the particles of $a = 4$ and rapidly decreases with a. The lift force can then be found from these calculations, by assuming that the particle motion is quasi-stationary. The lift is balanced by the $z-$ component of the drag, $F'_l = -F'_{dz}$. Following Dubov *et al.* (2014) we use an expression

$$F'_{dz} \approx -6\pi\mu a V'_m f_z(z/H, a/H), \tag{3.1}$$

$$f_z = 1 + \frac{a}{z-a} + \frac{a}{H-a-z}, \tag{3.2}$$

where the second and the third terms are corrections to the Stokes drag due to hydrodynamic interactions with two channel walls. In what follows

$$c_l = 6\pi V_m f_z \mathrm{Re}_p^{-1}. \tag{3.3}$$

Second method to calculate the lift (and to check the validity of the first approach) uses the balance of the lift and the gravity forces described by Equation (2.8). By varying the gravity force F_g one can, therefore, comprehend the whole range of equilibrium positions within the channel to obtain $c_l(z)$. The advantage of such an approach is that it does not require the particle motion to be quasi-stationary. However, the disadvantage of this method is that the convergence to equilibrium can be slow in the central zones of the channel, where the slope of $c_l(z)$ is small. Therefore, we use this computational strategy only in the near-wall region.

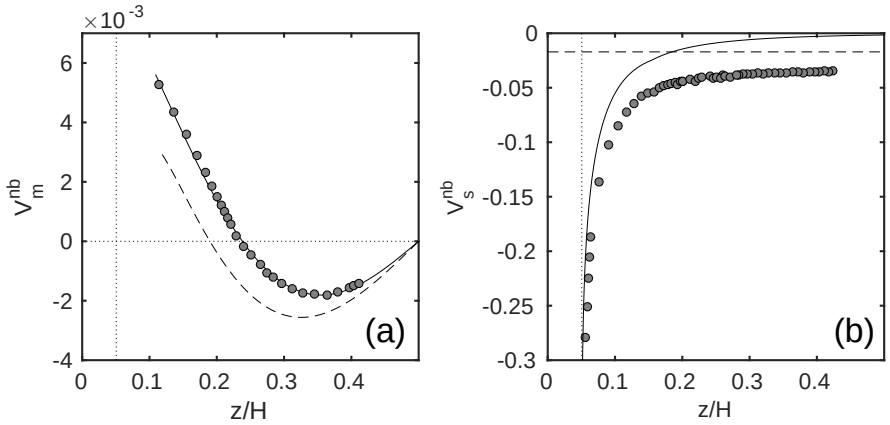

FIGURE 2. (a) Dimensionless migration velocity computed as a function of z/H for particles of $a = 4\delta$ (symbols). The location of the particle in a contact with the wall, $z = a$, is shown by a vertical dotted line. Dashed curve plots theoretical predictions for pointlike particles. Solid curve shows a polynomial fit of simulation data. (b) Dimensionless slip velocities computed for the same particles (symbols). Solid curve plots the slip velocity in a linear shear flow near a single wall. Dashed line plots the Faxen correction. Vertical dotted line indicates the location of $z = a$.

4. Results and discussion

In this section, we present the lattice Boltzmann simulation results and compare them with theoretical predictions.

4.1. *Neutrally buoyant particles*

We start with neutrally buoyant particles and first calculate their migration V_m^{nb} and the slip V_s^{nb} velocities as a function of z/H. Figure 2 plots simulation data obtained for particles of radius $a = 4\delta$. Here we show only a half of the channel since the curves are antisymmetric with respect to the channel axis $z = H/2$. These results demonstrate that migration velocity differs significantly from the velocity $c_{l0}\mathrm{Re}_p/(6\pi)$, where $\mathrm{Re}_p = a^2 G_m/\nu$, predicted theoretically for pointlike particles (Vasseur & Cox 1976). We also see that the equilibrium position, $V_m^{nb} = 0$, of finite-size particles is shifted towards the channel axis compared to that of pointlike particles, which is obviously due to their interactions with the wall resulting in a finite slip velocity. Indeed, Figure 2(b) demonstrates that computed V_s^{nb} grows rapidly near the wall being close to the theoretical predictions for a linear shear flow near a single wall (Goldman *et al.* 1967). Unlike theoretical predictions by Goldman *et al.* (1967), the computed slip velocity does not vanish in the central part of the channel. Its value is roughly twice larger than the Faxen correction $4U_m' a^2/(3H^2)$ (Happel & Brenner 1965). Note that a similar difference has been obtained in simulations of the migration of finite-size particles based on the Force Coupling Method (Loisel *et al.* 2015). These deviations from the Faxen corrections are likely also caused by hydrodynamic interactions of particles with the wall in a parabolic flow.

Figure 3 shows c_l for particles of $a = 4\delta$ and 8δ. The lift coefficient has been obtained from the migration velocity and from the force balance as specified above, and simulations have been made for two moderate Reynolds numbers, $\mathrm{Re} = 11.3$ and 22.6. As we discussed above, if $\mathrm{Re} \leq 20$ a potential dependence of c_l on Re could be ruled out *a priori*, and this is indeed confirmed by our simulations. Therefore, below we provide a detailed comparison of our simulation data with asymptotic solutions obtained for $\mathrm{Re} \ll 1$, which should be applicable for finite moderate Re. Figure 3 also includes theoretical predictions by Vasseur & Cox (1976) and curves calculated with Equation (2.5). One can see that simulation results show strong discrepancy from point-particle approximation, especially in the near-wall region, where hydrodynamic interactions are

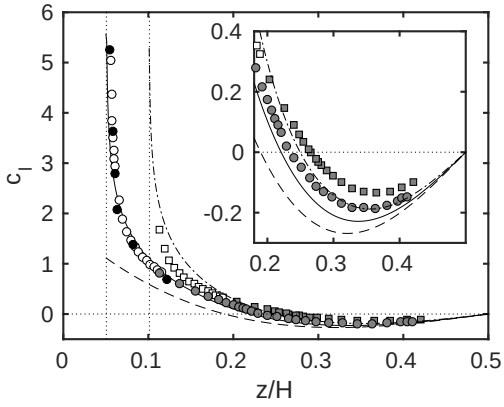

FIGURE 3. Lift coefficient, c_l, for neutrally buoyant particles of $a = 4\delta$ (circles) and 8δ (squares) obtained from the migration velocity at $\mathrm{Re} = 11.3$ (grey symbols) and 22.6 (white symbols). Solid and dash-dotted curves show predictions of Equation (2.5) for $a = 4\delta$ and 8δ, dashed curve plots predictions for point–like particles. Vertical dotted lines show $z = a$. Black symbols show c_l obtained for non-neutrally buoyant particles of $a = 4\delta$ from the force balance at $\mathrm{Re} = 22.6$. The inset plots c_l in the central part of the channel.

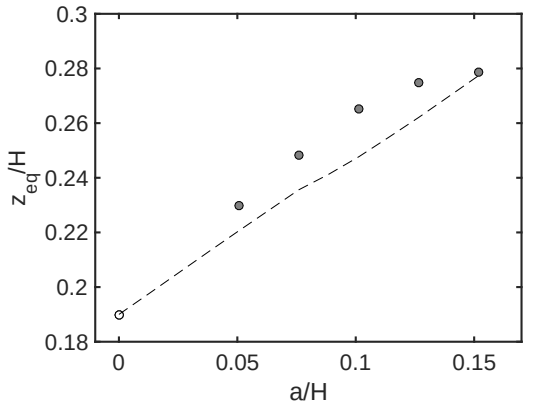

FIGURE 4. Equilibrium positions for neutrally buoyant finite-sized (gray circles) and point-like (white circle) particles. Dashed curve shows predictions of Equation (2.5).

significant. This discrepancy increases with the size of particles. We can, however, conclude that predictions of our Equation (2.5) are generally in good agreement with simulation results. Thus, for smaller particles, of $a = 4\delta$, Equation (2.5) perfectly fits the simulation data in the near-wall region, where the theory for point-like particles fails. Simulation results slightly deviate from predictions of Equation (2.5) near the equilibrium positions and in the central part of the channel. For bigger particles, of $a = 8\delta$, these deviations are more pronounced. We emphasize, however, that they are still much smaller than from the point-particle theory by Vasseur & Cox (1976).

To examine a significance of the particle size in more detail, we plot in Figure 4(a) computed equilibrium position, z_{eq}/H, as a function of a/H. We recall that the lift $c_l^{nb}(z)$ is antisymmetric with respect to the midplane of the channel axis, so that neutrally buoyant particles have a second equilibrium position at $H - z_{eq}$. In a point-particle approximation $z_{eq}/H \simeq 0.19$ (Vasseur & Cox 1976). We see that for finite-size particles z_{eq}/H is always larger, and increases with the particle size. Note that the increase in z_{eq}/H is nearly linear when $a/H \leq 0.1$. Also included in Figure 4

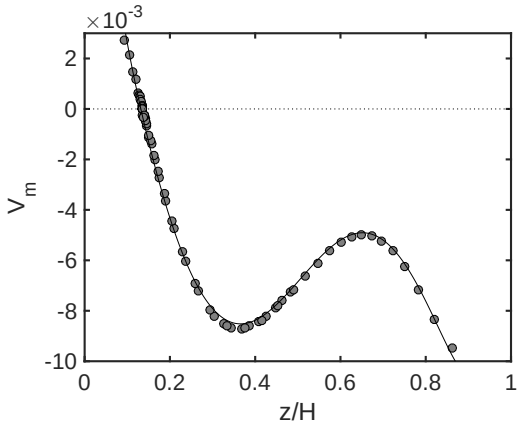

FIGURE 5. Migration velocity of non-neutrally buoyant particles in a horizontal channel. Symbols show simulation data. Solid curve is calculation with Equation (4.1) using data for neutrally buoyant particles.

are predictions of Equation (2.5). One can conclude that the theory correctly predicts the trend observed in simulations, but slightly deviates from the simulation data. A possible explanation for this discrepancy could be effects of parabolic flow (which are of the order of $O(a/H)$) on the slip velocity and the stresslet (see Yahiaoui & Feuillebois 2010; Hood *et al.* 2015), which are neglected in our theory.

4.2. *Non-neutrally buoyant particles*

We now turn to the particle migration under both inertial lift and gravity forces.

4.2.1. *Horizontal channel*

Let us start with the investigation of migration of particles in a most relevant experimentally case of a horizontal channel ($\alpha = 0^\circ$).

We first fix a weak gravity force, $F_g = 0.694$, and compute the migration velocity of particles of radii $a = 4\delta$ in a horizontal channel. Simulation results are plotted in Figure 5. We see that $V_m(z)$ is no longer antisymmetric, as it has been in the case of neutrally buoyant particles. The migration velocity can be calculated as

$$V_m = V_m^{nb} - V^{St}/f_z, \tag{4.1}$$

where we use a fit for V_m^{nb} computed for neutrally-buoyant particles (see Figure 2(a)). The agreement between simulation data and calculations using Equation (4.1) is excellent, which confirms that Equation (2.5) remains valid in the case of slightly non-neutrally buoyant particles. We remark that due to gravity V_m is shifted downwards relative to $V_m^{nb}(z)$ shown in Figure 2. As a result, with the taken value of F_g the second equilibrium position disappeared.

We recall that this type of simulations allows one to find values of $c_l(z)$ in the vicinity of the wall by varying F_g. We have included these force balance results in Figure 3 and can conclude that they agree very well with data obtained by using another computational method and for neutrally-buoyant particles. This suggests again that above results could be used at moderate Reynolds numbers, Re ≤ 20, since in this case the lift coefficient does not depend on Re.

Figure 6(a) shows z_{eq}/a computed at several F_g. It can be seen that when the gravity force is getting larger, the equilibrium positions decrease rapidly. This trend can be used to separate particles even when $\Delta\rho$ is very small. To illustrate this we now fix Re $= 11.3$, inject particles of $a = 4\delta$ close to the bottom of the channel, $z_0 = 1.125a$, and simulate their trajectories at different F_g. In Figure 6(b) we plot trajectories of particles, z/a, as a function of $xG_m a\nu$. The data show

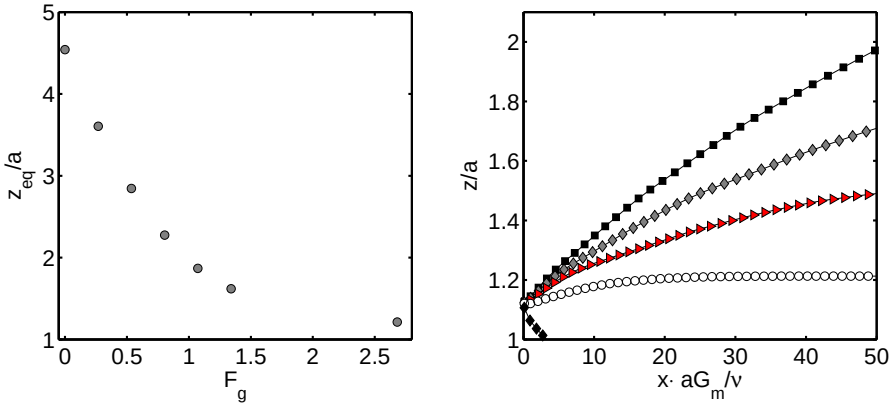

FIGURE 6. (a) Equilibrium positions of non-neutrally buoyant particles ($a = 4\delta$) in a horizontal channel; (b) trajectories of the same particles released at $z_0 = 1.125a$ computed at different $F_g = 0.268$ (squares), 0.804 (diamonds), 1.340 (triangles), 2.681 (circles), 9.383 (diamonds).

that if F_g is large enough, particles sediment to the wall. However, when F_g is relatively small, particles follow different and divergent trajectories, by approaching their equilibrium positions. We stress that at a given F_g and a/H trajectories, shown Figure 6(b), remain the same for any $\mathrm{Re} \leq 20$ (see Appendix B). Therefore, even in the case of very small $\Delta\rho$, one can always tune the value of Re to induce the required for separation difference in F_g. For example, we have to separate particles of $a = 2$ μm and different $\Delta\rho$ in the channel of $H = 40$ μm. If we chose $\mathrm{Re} = 0.3$, the separation length $L = 50 x G_m a \nu$ of Figure 6(b) will be ca. 3.3 cm. By evaluating $\Delta\rho$ with Equation (2.6), we can immediately conclude that trajectories plotted in Figure 6(b) from top to bottom correspond to $\Delta\rho = 0.007$, 0.022, 0.037 and 0.073, which is indeed extremely small.

4.2.2. *Inclined channel*

When F_g is large enough, it can also influences the slip velocity, and therefore, change the lift itself. This effect is especially important for vertical channels. Note that due to the linearity of the Stokes equations, which govern a disturbance flow at small particle Reynolds numbers, we can decouple the contributions of the particle-wall interaction and of the gravity force into the slip velocity:

$$V_s = V_s^{nb} + \Delta V_s \sin\alpha, \tag{4.2}$$

where $\Delta V_s = V^{St}/f_x$ is the gravity-induced slip velocity for a vertical channel ($\alpha = 90^\circ$) and $f_x(z/H, a/H)$ is the correction to the drag for a particle translating parallel to the channel walls. The slip and the migration velocities of particles of $a = 4\delta$ in a vertical channel computed by using several values of F_g are shown in Figures 7(a) and 8(a). Note that the slip velocity, V_s, grows with F_g since the Stokes velocity, V^{St}, is linearly proportional to F_g (see Eq.(2.7)). We now use simulation data presented in Figures 2(a) and 7(a) to compute ΔV_s, and then $\Delta V_s/F_g$. The results for $\Delta V_s/F_g$ are shown in Figure 7(b), and we see that all data collapse into a single curve, which confirms the validity of Equation (4.2). Figure 7(b) also shows that $\Delta V_s/F_g$ is nearly constant in the central region of the channel, being smaller than V^{St}, but the deviations from V^{St} grow when particles approach the wall. These results again illustrate that hydrodynamic interactions with the walls significantly affect motion of particles in the channel.

We recall that the variation of the slip velocity caused by gravity is small for slightly non-

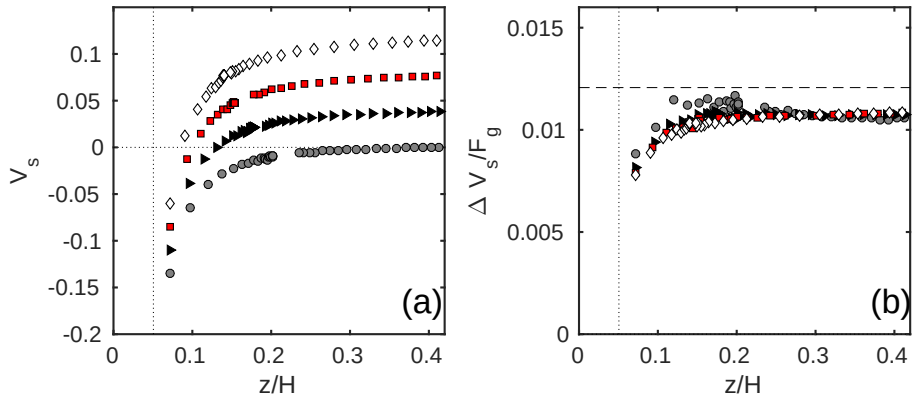

FIGURE 7. Slip velocities (a) and $\Delta V_s/F_g$ (b) computed for non-neutrally buoyant particles of $a = 4\delta$ in a vertical channel. The data sets correspond to $F_g = 3.475$ (circles), 6.956 (triangles), 10.44 (squares) and 13.91 (diamonds). Dashed line shows V^{St}/F_g, vertical dotted lines plot $z = a$.

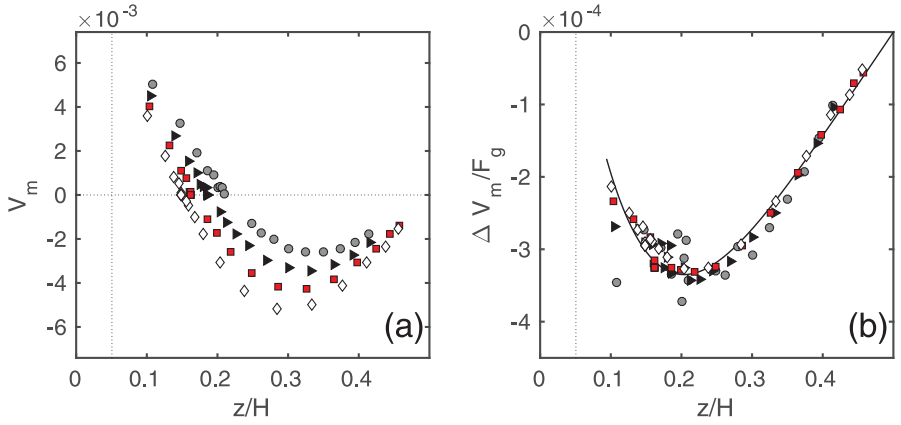

FIGURE 8. Migration velocities (a) and $\Delta V_m/F_g$ (b) computed for non-neutrally buoyant particles of $a = 4\delta$ in a vertical channel. The data sets correspond to $F_g = 3.475$ (circles), 6.956 (triangles), 10.44 (squares) and 13.91 (diamonds). Vertical dotted lines plot $z = a$. Solid curve shows a polynomial fit of data.

neutrally buoyant particles (see Figure 7), so that Eq.(2.5) can be linearized with respect to ΔV_s:

$$c_l \simeq c_l^{nb} + \Delta V_s \frac{\partial c_l(V_s^{nb})}{\partial V_s}, \tag{4.3}$$

where $c_l^{nb} = c_l(V_s^{nb})$ is the lift coefficient for neutrally buoyant particles. By using Eq.(3.3) we can then calculate the migration velocity

$$V_m = V_m^{nb} + \Delta V_m = V_m^{nb} + \Delta V_s \frac{\partial c_l(V_s^{nb})}{\partial V_s} \frac{\mathrm{Re}_p}{6\pi f_z}. \tag{4.4}$$

The computed migration velocity is shown in Figure 8(a). We see that it decreases with F_g, and the equilibrium position shifts towards the wall, which is since $\Delta V_s/F_g$ is positive while $\partial c_l/\partial V_s$ is negative.

We can now evaluate $\Delta V_m/F_g$ by using simulation data presented in Figures 2 and 8(a), and these results are presented in Figure 8(b). As one can see, the data collapse into a single curve, thus confirming the validity of our linearization, Equation (4.4).

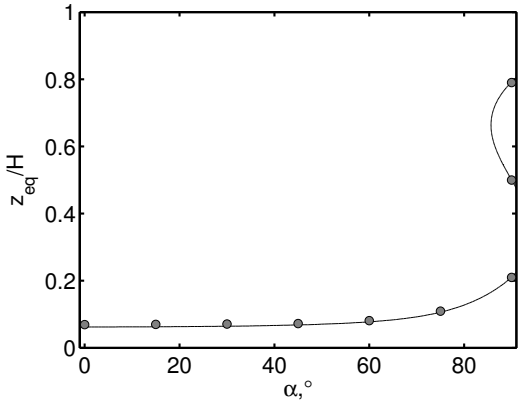

FIGURE 9. Equilibrium positions z_{eq}/H for $a = 4\delta$ and $F_g = 3.475$. Circles show simulation data. Solid curve plots results obtained using $V_m = 0$, where V_m is calculated with Eq. (4.6).

Finally, we briefly discuss the case of an arbitrary inclination angle α, where the z-component of the force can be written as

$$F_z = c_l(V_s) + F_g \cos\alpha. \tag{4.5}$$

By using Eqs.(4.2), (4.4) and (4.5), we can express the migration velocity as

$$V_m = V_m^{nb} + \Delta V_m \sin\alpha + F_g \cos\alpha \frac{\mathrm{Re}_p}{6\pi f_z}, \tag{4.6}$$

where ΔV_m is evaluated for a vertical channel (see Figure 8(b)). The equilibrium positions can be found by using a condition $V_m = 0$, where V_m is calculated with Eq.(4.6). The results of these calculations made at a fixed $F_g = 3.475$ and different α are plotted in Figure 9 together with direct simulation data, and one can see that they practically coincide. Our results show that in a vertical channel two stable equilibrium positions coexist. They are symmetric relative to the midplane and are located close to walls. Another, third equilibrium position has a locus at the midplane, but is unstable. A similar result has been obtained earlier (Vasseur & Cox 1976; Asmolov 1999). If we slightly reduce α both stable equilibrium positions become shifted towards the lower wall due to gravity as well seen in Figure 9. These two positions coexist only for $\alpha \geq 85.7^\circ$. On reducing α further the upper equilibrium position disappears, and only one, a lower, equilibrium position remains. This obviously indicates that the inertial lift cannot balance gravity anymore. We note that this remaining single equilibrium position becomes insensitive to the inclination angle when $\alpha \leq 60^\circ$.

5. Concluding remarks

In this paper we have studied the inertial migration of finite-size particles in a plane channel flow at moderate Reynolds numbers, $\mathrm{Re} \leq 20$. We have shown that the slip velocity, V_s, which is finite even for neutrally buoyant particles, contributes to the lift and determines the equilibrium positions in the channel. We have proposed an expression for the lift which generalizes theories, originally applied for some cases of limited guidance, to finite-size particles in a channel flow. When the size of particle turns to zero, our formula recovers known expression of a point-particle approximation (Vasseur & Cox 1976). For particles close to the walls we recover earlier predictions for finite-size particles in a linear shear flow (Cherukat & Mclaughlin 1994). Our theoretical model, which is probably the simplest realistic model for a lift in the channel that one might contemplate, provides considerable insight into inertial migration of finite-size particles in

microchannels. In particular, it provides a simple explanation of a significant increase in the lift near walls. It also allows one to predict a number of equilibrium positions and determine their location in various situations.

To check the validity of our theory, we have employed lattice Boltzmann simulations. Generally, the simulation results have fully confirmed the theory, and have shown that many of our theoretical results have validity beyond initial restrictions of our model. Thus, it has been confirmed that predictions of our theory do not depend on Reynolds number when $\mathrm{Re} \leq 20$, that equilibrium positions of heavy particles in a horizontal channel can be accurately determined by using data for the neutrally buoyant case, and more.

Several of our theoretical predictions could be tested in experiment. In particular, we have shown that particles of a very small density contrast should follow divergent trajectories, so that channel flows with low Reynolds numbers $\mathrm{Re} \sim 1$ can be used to separate such particles. We stress that our theory should correctly predict the lift in near-wall regions also in pipes or square channels, and we expect that for this geometry it could be accurate even at $\mathrm{Re} \geq 20$ since the lengthscale of the disturbance flow would rather be the distance to the wall than the channel width. By this reason it would be possible to neglect the effects of other distant walls and parabolic flow on the lift. Note, however, that these effects should be taken into account in the central part of the channel.

Our model and computational approach can be extended to more complex situations, which include, for example, hydrophobic walls or particles allowing hydrodynamic slip at their surfaces (Vinogradova 1999; Neto *et al.* 2005). In this case the hydrodynamic interaction in the near-wall region changes significantly (Davis *et al.* 1994; Vinogradova 1996), so that we expect that the lift force can be also dramatically modified. It would also be interesting to consider a case of an anisotropic superhydrophobic wall, which could induce secondary flows transverse to the direction of applied pressure gradient (Feuillebois *et al.* 2010; Vinogradova & Belyaev 2011; Schmieschek *et al.* 2012). It has been recently shown (Asmolov *et al.* 2015; Pimponi *et al.* 2014) that particles translating in a superhydrophobic channel can be laterally displaced due to such a transverse flow. The use of this effect in combination with the inertial migration should be a fruitful direction, which could allow to separate particles of different size or density contrast not only by their vertical but also by transverse positions.

We thank Sebastian Schmieschek and Manuel Zellhöfer for their help on technical aspects of the simulations. This research was partly supported by the Russian Foundation for Basic Research (grant 15-01-03069).

Appendix A. Fits for the slip velocity and the lift coefficients

In this Appendix we summarize known results for the slip velocity and the lift coefficients for finite-size particles in a linear shear flow near a single wall and for point-like particles in a Poiseuille flow. The velocity of a freely translating and rotating particle in a linear shear flow is given by (Goldman *et al.* 1967)

$$V_x^{nb'} = U'(z)\, h, \tag{A 1}$$

where h is the correction function which depends on z/a only. We use (A 1) to estimate the slip velocity in channel flow, i.e., we neglect the effects due to parabolic flow, so that

$$V_s^{nb} = \frac{z(H-z)(h-1)}{aH}. \tag{A 2}$$

The correction factor fitting the results by Goldman *et al.* (1967) in the near-wall region reads (Reschiglian *et al.* 2000)

$$h = \frac{200.9b - (115.7b + 721)\zeta^{-1} - 781.1}{-27.25b^2 + 398.4b - 1182} \quad \text{at} \quad \zeta < 3, \tag{A 3}$$

where $\zeta = z/a$ and $b = \log(\zeta - 1)$. Note that here we have reformulated the original equation (Reschiglian *et al.* 2000) in terms of the natural logarithm. For larger distances we use the asymptotic solution by Wakiya *et al.* (1967),

$$h = \frac{1 - \frac{5}{4}\zeta^{-3} + \frac{5}{4}\zeta^{-5} - \frac{23}{48}\zeta^{-7} - \frac{1375}{1024}\zeta^{-8}}{1 - \frac{15}{16}\zeta^{-3} + \zeta^{-5} - \frac{3}{8}\zeta^{-7} - \frac{4565}{4096}\zeta^{-8}} \quad \text{at} \quad \zeta \geq 3. \tag{A 4}$$

Vasseur & Cox (1976) have obtained the lift force on a particle in a channel flow at $\mathrm{Re} \ll 1$ by using a point-particle approximation:

$$c_l^{VC} = c_{l0}^{VC} + \frac{H}{a} c_{l1}^{VC} V_s + c_{l2}^{VC} V_s^2, \tag{A 5}$$

where coefficients $c_{l0}^{VC}, c_{l1}^{VC}, c_{l2}^{VC}$ depend on z/H only. Later Feuillebois (2004) has proposed a simple fitting expression:

$$c_{l0}^{VC} = 2.25\,(z/H - 0.5) - 23.4\,(z/H - 0.5)^3\,. \tag{A 6}$$

The expression for a lift coefficient of a finite-size particle in a linear shear flow near a single wall has been suggested by Cherukat & Mclaughlin (1994)

$$c_l^{CM} = c_{l0}^{CM} + c_{l1}^{CM} V_s + c_{l2}^{CM} V_s^2, \tag{A 7}$$

where the coefficients $c_{l0}^{CM}, c_{l1}^{CM}, c_{l2}^{CM}$ depend on ζ only:

$$c_{l0}^{CM} = 1.8081 + 0.879585\zeta^{-1} - 1.9009\zeta^{-2} + 0.98149\zeta^{-3}, \tag{A 8}$$

$$c_{l1}^{CM} = -3.24139\zeta - 2.676 - 0.8248\zeta^{-1} + 0.4616\zeta^{-2}, \tag{A 9}$$

$$c_{l2}^{CM} = 1.7631 + 0.3561\zeta^{-1} - 1.1837\zeta^{-2} + 0.845163\zeta^{-3}. \tag{A 10}$$

Appendix B. Governing equations for trajectories of particles

In this Appendix, we derive equations which govern particle trajectories. The components of the particle velocity can be written as

$$\frac{dx}{dt} = V_x' = U'(z)\,h = G_m z (1 - z/H) h, \tag{B 1}$$

$$\frac{dz}{dt} = V_m' = \frac{F_l' - F_g'}{6\pi\mu a f_z} = \frac{(c_l - F_g)\,a^3 G_m^2}{6\pi\nu f_z}. \tag{B 2}$$

The last equality indicates that the migration time, i.e., the time required for a particle to migrate at distance of the order of its radius a, is equal to $\nu/(G_m a)^2 = (4G_m\mathrm{Re})^{-1}(H/a)^2$. Since the right-hand sides of (B 1) and (B 2) do not explicitly include time, one can formulate an equation governing the particle trajectory as

$$\frac{dz}{dx} = \frac{a^3 G_m}{6\pi\nu} \frac{c_l - F_g}{f_z z (1 - z/H) h}. \tag{B 3}$$

Let us now turn to dimensionless coordinates ζ and $\xi = x G_m a/\nu$. Equation (B 3) can then be

rewritten as

$$\frac{d\zeta}{d\xi} = \frac{1}{6\pi} \frac{c_l - F_g}{f_z h \zeta (1 - \zeta a/H)}. \tag{B 4}$$

We stress that Equation (B 4) does not depend on Re. Indeed, f_z and h are dimensionless functions of ζ and a/H only, and the lift coefficient, c_l, is also not sensitive to the Reynolds number when $\mathrm{Re} \leq 20$. This implies that at given F_g and a/H trajectories satisfying Equation (B 4) are universal, i.e. remain the same at any $\mathrm{Re} \leq 20$.

REFERENCES

ASMOLOV, E. S. 1999 The inertial lift on a spherical particle in a plane Poiseuille flow at large channel Reynolds number. *J. Fluid Mech.* **381**, 63–87.

ASMOLOV, E. S., DUBOV, A. L., NIZKAYA, T. V., KUEHNE, A. J. C. & VINOGRADOVA, O. I. 2015 Principles of transverse flow fractionation of microparticles in superhydrophobic channels. *Lab. Chip* **15** (13), 2835–2841.

BENZI, R., SUCCI, S. & VERGASSOLA, M. 1992 The lattice Boltzmann equation: theory and applications. *Physics Reports* **222**, 145.

BHAGAT, A.A.S., KUNTAEGOWDANAHALLI, S.S. & PAPAUTSKY, I. 2008 Continuous particle separation in spiral microchannels using dean flows and differential migration. *Lab. Chip* **8** (11), 1906–1914.

CHERUKAT, P. & MCLAUGHLIN, J. B. 1994 The inertial lift on a rigid sphere in a linear shear flow field near a flat wall. *J. Fluid Mech.* **263**, 1–18.

CHOI, Y.-S., SEO, K.-W. & LEE, S.-J. 2011 Lateral and cross-lateral focusing of spherical particles in a square microchannel. *Lab. Chip* **11** (3), 460–465.

CHUN, B. & LADD, A. J. C. 2006 Inertial migration of neutrally buoyant particles in a square duct: An investigation of multiple equilibrium positions. *Phys. Fluids* **18**, 031704.

COX, R. G. & HSU, S. K. 1977 The lateral migration of solid particles in a laminar flow near a plane. *Int. J. Multiph. Flow* **3**, 201–222.

DAVIS, A. M. J., KEZIRIAN, M. T. & BRENNER, H. 1994 On the Stokes-Einstein model of surface diffusion along solid surfaces: Slip boundary conditions. *J. Colloid Interface Sci.* **165** (1), 129–140.

DI CARLO, D., EDD, J. F., HUMPHRY, K. J., STONE, H. A. & TONER, M. 2009 Particle segregation and dynamics in confined flows. *Phys. Rev. Lett.* **102** (9), 094503.

DI CARLO, D., IRIMIA, D., TOMPKINS, R.G. & TONER, M. 2007 Continuous inertial focusing, ordering, and separation of particles in microchannels. *Proc. Natl. Acad. Sci. U.S.A.* **104** (48), 18892–18897.

DUBOV, A. L., SCHMIESCHEK, S., ASMOLOV, E. S., HARTING, J. & VINOGRADOVA, O. I. 2014 Lattice-Boltzmann simulations of the drag force on a sphere approaching a superhydrophobic striped plane. *J. Chem. Phys.* **140** (3), 034707.

DUTZ, S., HAYDEN, M.E. & HÄFELI, U.O. 2017 Fractionation of magnetic microspheres in a microfluidic spiral: Interplay between magnetic and hydrodynamic forces. *PLOS ONE* **12** (1), e0169919.

FEUILLEBOIS, F. 2004 Perturbation problems at low Reynolds number. *Lecture Notes-AMAS* .

FEUILLEBOIS, F., BAZANT, M. Z. & VINOGRADOVA, O. I. 2010 Transverse flow in thin superhydrophobic channels. *Phys. Rev. E* **82**, 055301(R).

GOLDMAN, A. J., COX, R. G. & BRENNER, H. 1967 Slow viscous motion of a sphere parallel to a plane wall - II Couette flow. *Chem. Eng. Sci.* **22**, 653–660.

HAPPEL, J. & BRENNER, H. 1965 Low Reynolds number hydrodynamics with special applications to particulate media. *Prentice-Hall* .

HARTING, J., FRIJTERS, S., RAMAIOLI, M., ROBINSON, M., WOLF, D. E. & LUDING, S. 2014 Recent advances in the simulation of particle-laden flows. *Eur. Phys. J. Spec. Topics* **223**, 2253–2267.

HO, B.P. & LEAL, L.G. 1974 Inertial migration of rigid spheres in two-dimensional unidirectional flows. *J. Fluid Mech.* **65**, 365–400.

HOOD, K., KAHKESHANI, S., DI CARLO, D. & ROPER, M. 2016 Direct measurement of particle inertial migration in rectangular microchannels. *Lab. Chip* **16**, 2840–2850.

HOOD, K., LEE, S. & ROPER, M. 2015 Inertial migration of a rigid sphere in three-dimensional Poiseuille flow. *J. Fluid Mech.* **765**, 452–479.

JANOSCHEK, F. 2013 Mesoscopic simulation of blood and general suspensions in flow. *Eindhoven University of Technology (Ph. D. thesis)* .

JANOSCHEK, F., TOSCHI, F. & HARTING, J. 2010 Simplified particulate model for coarse-grained hemodynamics simulations. *Phys. Rev. E* **82**, 056710.

KILIMNIK, A., MAO, W. & ALEXEEV, A. 2011 Inertial migration of deformable capsules in channel flow. *Phys. of Fluids* **23** (12), 123302.

KRISHNAN, G. P. & LEIGHTON JR., D. T. 1995 Inertial lift on a moving sphere in contact with a plane wall in a shear flow. *Phys. Fluids* **7** (11), 2538–2545.

KUNERT, C., HARTING, J. & VINOGRADOVA, O. I. 2010 Random-roughness hydrodynamic boundary conditions. *Phys. Rev. Lett.* **105** (1), 016001.

LADD, A. J. C. & VERBERG, R. 2001 Lattice-Boltzmann simulations of particle-fluid suspensions. *J. Stat. Phys.* **104** (5), 1191.

LIU, C., HU, G., JIANG, X. & SUN, J. 2015 Inertial focusing of spherical particles in rectangular microchannels over a wide range of Reynolds numbers. *Lab. Chip* **15** (4), 1168–1177.

LIU, C., XUE, C., SUN, J. & HU, G. 2016 A generalized formula for inertial lift on a sphere in microchannels. *Lab. Chip* **16** (5), 884–892.

LOISEL, V., ABBAS, M., MASBERNAT, O. & CLIMENT, E. 2015 Inertia-driven particle migration and mixing in a wall-bounded laminar suspension flow. *Phys. Fluids* **27** (12), 123304.

MARTEL, J. M. & TONER, M. 2014 Inertial focusing in microfluidics. *Annu. Rev. Biomed. Eng.* **16**, 371–396.

MATAS, J.-P., MORRIS, J. F. & GUAZZELLI, E. 2004 Inertial migration of rigid spherical particles in Poiseuille flow. *J. Fluid Mech.* **515**, 171–195.

MATAS, J.-P., MORRIS, J. F. & GUAZZELLI, E. 2009 Lateral force on a rigid sphere in large-inertia laminar pipe flow. *J. Fluid Mech.* **621**, 59–67.

MIURA, K., ITANO, T. & SUGIHARA-SEKI, M. 2014 Inertial migration of neutrally buoyant spheres in a pressure-driven flow through square channels. *J. Fluid Mech.* **749**, 320–330.

MORITA, Y., ITANO, T. & SUGIHARA-SEKI, M. 2017 Equilibrium radial positions of neutrally buoyant spherical particles over the circular cross-section in Poiseuille flow. *J. Fluid Mech.* **813**, 750–767.

NETO, C., EVANS, D., BONACCURSO, E., BUTT, H. J. & CRAIG, V. J. 2005 Boundary slip in newtonian liquids: a review of experimental studies. *Rep. Prog. Phys.* **68**, 2859–2897.

PASOL, L., SELLIER, A. & FEUILLEBOIS, F. 2006 A sphere in a second degree polynomial creeping flow parallel to a wall. *QJ Mech. Appl. Math.* **59** (4), 587–614.

PIMPONI, D., CHINAPPI, M., GUALTIERI, P. & CASCIOLA, C. M. 2014 Mobility tensor of a sphere moving on a superhydrophobic wall: application to particle separation. *Microfluidics Nanofluidics* **16**, 571–585.

RESCHIGLIAN, P., MELUCCI, D., TORSI, G. & ZATTONI, A. 2000 Standardless method for quantitative particle-size distribution studies by gravitational field-flow fractionation. application to silica particles. *Chromatographia* **51** (1-2), 87–94.

SAFFMAN, P. G. 1965 The lift on a small sphere in a slow shear flow. *J. Fluid Mech.* **22**, 385–400.

SCHMIESCHEK, S., BELYAEV, A. V., HARTING, J. & VINOGRADOVA, O. I. 2012 Tensorial slip of superhydrophobic channels. *Phys. Rev. E* **85**, 016324.

SCHONBERG, J. A. & HINCH, E. J. 1989 Inertial migration of a sphere in Poiseuille flow. *J. Fluid Mech.* **203**, 517–524.

SEGRÉ, G. & SILBERBERG, A. 1962 Behaviour of macroscopic rigid spheres in Poiseuille flow. Part 2. Experimental results and interpretation. *J. Fluid Mech.* **14**, 136–157.

VASSEUR, P. & COX, R. G. 1976 The lateral migration of a spherical particle in two-dimensional shear flows. *J. Fluid Mech.* **78**, 385–413.

VINOGRADOVA, O. I. 1996 Hydrodynamic interaction of curved bodies allowing slip on their surfaces. *Langmuir* **12**, 5963–5968.

VINOGRADOVA, O. I. 1999 Slippage of water over hydrophobic surfaces. *Int. J. Miner. Proc.* **56**, 31–60.

VINOGRADOVA, O. I. & BELYAEV, A. V. 2011 Wetting, roughness and flow boundary conditions. *J. Phys.: Condens. Matter* **23**, 184104.

WAKIYA, S., DARABANER, C.L. & MASON, S.G. 1967 Particle motions in sheared suspensions XXI: Interactions of rigid spheres (theoretical). *Rheol. Acta* **6** (3), 264–273.

YAHIAOUI, S. & FEUILLEBOIS, F. 2010 Lift on a sphere moving near a wall in a parabolic flow. *J. Fluid Mech.* **662**, 447–474.

ZHANG, J., YAN, S., ALICI, G., NGUYEN, N.-T., DI CARLO, D. & LI, W. 2014 Real-time control of inertial focusing in microfluidics using dielectrophoresis (dep). *RSC Adv.* **4** (107), 62076–62085.

ZHANG, J., YAN, S., YUAN, D., ALICI, G., NGUYEN, N.-T., WARKIANI, M. E. & LI, W. 2016 Fundamentals and applications of inertial microfluidics: a review. *Lab. Chip* **16** (1), 10–34.